AIAA JOURNAL
Vol. 47, No. 10, October 2009

# Exploring Mechanisms of Fluidic Thrust Vectoring Using a Transverse Jet and Suction

D. J. Forliti* and I. Echavarria Diaz-Guardamino†
*University at Buffalo, State University of New York, Buffalo, New York, 14260*

DOI: 10.2514/1.39063

**Fluidic flow control methods, such as transverse injection or suction, have been shown to be effective for thrust vector angle control of the flow issuing from a rectangular channel. The Reynolds number based on the channel height was 39,000. The objective of the current work was to explore the operating mechanism of these independent fluidic approaches and to consider the performance when they are combined in a single configuration. Suction vectors the flow via static pressure control near the jet exit, where the pressure boundary condition extends into the channel to produce finite vectoring at the exit of the jet. Transverse injection within the channel produces a recirculation zone that contributes to the vectoring effect due to the alteration of the wall static pressure distribution. The influence of suction on the vectoring performance is dependent on the level of transverse injection, with a degraded suction effect at higher transverse injection rates. Suction is effective when it is able to disturb and enhance the mixing of the jet shear layer.**

## Nomenclature

| | | |
|---|---|---|
| $C_q$ | = | suction mass flow ratio |
| $C_\mu$ | = | momentum ratio |
| $d$ | = | injection slot thickness |
| $H$ | = | channel height |
| $h$ | = | suction slot height |
| $L$ | = | distance between injection and the end of the channel |
| $M_x$ | = | streamwise momentum transport across the channel cross section |
| $M_y$ | = | cross-stream momentum transport across the channel cross section |
| $\dot{m}$ | = | mass flow rate |
| $P$ | = | static pressure |
| $U$ | = | mean streamwise velocity |
| $u'$ | = | streamwise velocity fluctuation |
| $V$ | = | mean cross-stream velocity |
| $v'$ | = | cross-stream velocity fluctuation |
| $x$ | = | streamwise coordinate |
| $y$ | = | cross-stream coordinate |
| $\alpha$ | = | thrust vector angle |
| $\delta$ | = | 99% boundary-layer thickness |
| $\lambda$ | = | shear layer velocity ratio parameter |
| $\rho$ | = | density |

*Subscripts*

| | | |
|---|---|---|
| $j$ | = | jet flow |
| $s$ | = | suction flow |
| 0 | = | channel flow |

## I. Introduction

WEIGHT reduction, stealth, and air superiority are considered to be the main focuses of modern defense aerospace research. One emerging technology, thrust vector control, provides the aircraft with enhanced maneuverability and a broadened flight envelope while at the same time offering the potential for reduction of aerodynamic surfaces that contribute to drag and radar signature.

The thrust vectoring concept is based on the alteration of the force balance of the aircraft propulsive system, providing the necessary conditions for rapid changes in attitude. Present technologies create this alteration through the use of mechanical actuators and vanes that modify the shape of the exhaust nozzle and induce a change in the exhaust stream direction. However, the complexity of these mechanical systems and the need to protect the components from harmful conditions induce substantial weight, maintenance, and design constraints. To avoid these major drawbacks, attention has been focused on the development of fixed-geometry thrust vectoring systems that employ fluidic flow control. Fluidic thrust vectoring methods typically rely on injection, suction, or controlled excitation of the flow to produce the vectoring effect.

A variety of injection-based thrust vectoring schemes have been developed. Shock-vector control is one of the oldest thrust vectoring approaches developed to control supersonic jets using transverse jet injection [1]. In recent years, injection-based methods have been considered that do not rely on shock waves for flow turning. To eliminate the penalties associated with the shock, Miller et al. [2] developed a technique that subsonically deflects the flow. The "throat skewing technique" achieves the jet deflection through asymmetrical injection into the throat as well as near the exit on the opposite wall of a convergent–divergent nozzle, resulting in a reorientation of the sonic line and, thus, a turning of the jet. The throat skewing concept was later used by Deere et al. [3] and Flamm et al. [4,5] as the baseline to develop the "dual throat" thrust vectoring nozzle concept. This new concept featured a convergent–divergent–convergent nozzle equipped with injection ports at the upstream throat, similar to that for the throat skewing concept. Injection can also be used in conjunction with confinement to manipulate the Coanda effect for thrust vector control [6,7].

Although transverse injection directly impacts the momentum within the nozzle, the flowfield created as the jet interacts with the main flow influences the static pressure along the wall of the nozzle. Weston and Thames [8] documented the wall pressure distribution produced for an unconfined transverse rectangular jet. It was found that the jet creates a region of positive gauge pressure upstream of the jet due to the blockage produced by the jet fluid to the crossflow.

The results of Weston and Thames provide guidance as to why the fluidic throat skewing thrust vectoring method works [2,9]. The streamwise offsetting of the control jets results in an overlapping region where the pressure along one wall is reduced while the pressure along the opposite wall is increased, due to the relative

Presented as Paper 3879 at the 4th AIAA Flow Control Conference, Seattle, WA, 23–26 June 2008; received 12 June 2008; revision received 3 June 2009; accepted for publication 30 June 2009. 

*Assistant Professor, Department of Mechanical and Aerospace Engineering, 312 Jarvis Hall. Senior Member AIAA.

†Graduate Student, Department of Mechanical and Aerospace Engineering, 312 Jarvis Hall. Student Member AIAA.

placement of the jets. This results in a large cross-stream pressure drop that produces vectored flow issuing from the nozzle. The role of compressibility and divergence on the static pressure control using transverse jets has not yet been documented.

Suction is a fluidic technique that has been employed in different configurations for thrust vectoring. Suction-based methods fall into two categories: turbulence control and local pressure control. The suction-based countercurrent shear thrust vectoring method was developed by Strykowski and Krothapalli [10] for sub- and supersonic jets. The counterflow thrust vectoring concept uses a secondary countercurrent flow along a suction collar (i.e., confinement surface) to excite the jet shear layer and create the pressure gradients required to vector the thrust. It has been shown that the enhanced turbulence of the countercurrent shear flow contributes to the vectoring mechanism when the jet is within close proximity to the confinement surface [11]. The concept was successfully implemented for realistic conditions [12,13] and provided a linear control of the deflection angle outside of the bistable regime associated with jet attachment to the collar.

The synthetic jet approach developed by Smith and Glezer [14] is a way of vectoring a jet using a zero-net mass flux device. For this concept, a synthetic jet actuator is located parallel to one of the *unconfined* shear layers along the long dimension of a rectangular jet. Operation of the synthetic jet actuator resulted in a vectoring of the flow toward the synthetic jet side. The synthetic jet lowers the pressure on the nearest side of the jet, and the pressure boundary condition extends into the channel, producing a vectored jet at the channel exit plane.

Combined suction and blowing were used by Bettridge et al. [15] to produce a steady effect similar to that induced using a synthetic jet. A suction slot was placed near the primary jet, and a blowing slot was placed next to the suction slot. Similar to the synthetic jet method, the role of the fluidics was to nominally control the static pressure distribution near the exit plane of the jet. The role of the blowing jet is to restrict free entrainment of ambient air into the suction slot; the apparent success of suction-based vectoring requires that the suction slot entrain fluid from the primary jet. This vectoring method has also been used for segregating particles based on diameter for characterization of polydisperse aerosols [16].

Suction applied to the blunt trailing edge of a planar jet in coflow was also studied by Lim and Redekopp [17] for thrust vectoring. The control of the jet angle was associated with the suction flow causing a suppression of global instability of the wake of the blunt trailing edge. The velocity profiles entering the blunt trailing edge were asymmetric, that is, likely to produce asymmetric primary jet entrainment into the suction slot.

It is clear that injection and suction have been independently applied to successfully achieve thrust vector angle control of jets. The goal of the present work was to study the thrust vectoring mechanisms of transverse injection and suction and explore the performance of combining these two fluidic approaches.

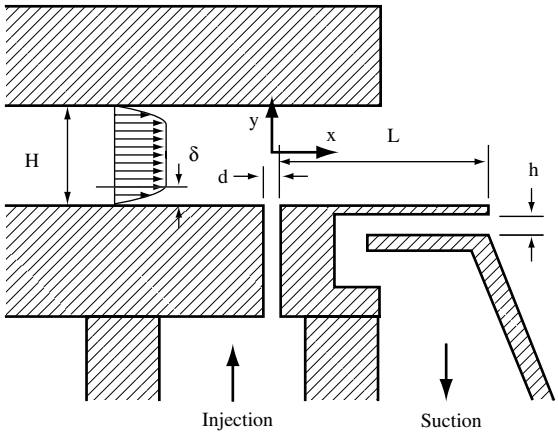


**Fig. 1 Schematic of the test section.**

## II. Experimental Setup

The experiments were conducted at the Combustion Laboratory in the Mechanical and Aerospace Engineering Department at the State University of New York at Buffalo. The air for the main channel flow is provided using a blowdown-type facility, in which pressurized air is regulated and supplied to a plenum containing flow conditioning elements. The transverse injection flow is supplied using building compressed air. The injection and suction flow rates are metered using rotameters. A Laskin nozzle is used to produce seed particles for particle image velocimetry (PIV). The suction flow is generated using a regenerative blower, and the suction flow rate applied to the test section is controlled with a bleed valve.

The test section, shown in Fig. 1, consists of a rectangular channel flow facility with a nominal aspect ratio of 4:1 and a short dimension $H$ of 12.1 mm. The injection and suction slots span 100% of the channel depth. The geometrical parameters were fixed, and no optimization was conducted. The injection port has a slot width $d$ of 1.2 mm, and flow conditioning inside the port ensured uniformity in the spanwise dimension; uniformity of the injection flow was verified using a spanwise profile measurement in the slot jet cross section. The suction slot has a uniform height $h$ of 1 mm. The suction flow enters a suction chamber that is placed between the suction slot and the manifold that is connected to the suction pump. The streamwise distance between the injection location and the end of the channel $L$ is $1.49H$. The origin of the coordinate system is located above the slot jet in the transverse and spanwise center of the channel.

Figure 2 shows profiles of the mean and rms of the fluctuation of the streamwise velocity near the injection point. The main flow had a top-hat velocity profile with a mean velocity of 50 m/s and background turbulence intensity in the core of approximately 1%. The Reynolds number based on the channel height and mean velocity was approximately 39,000. The boundary layers were approximately

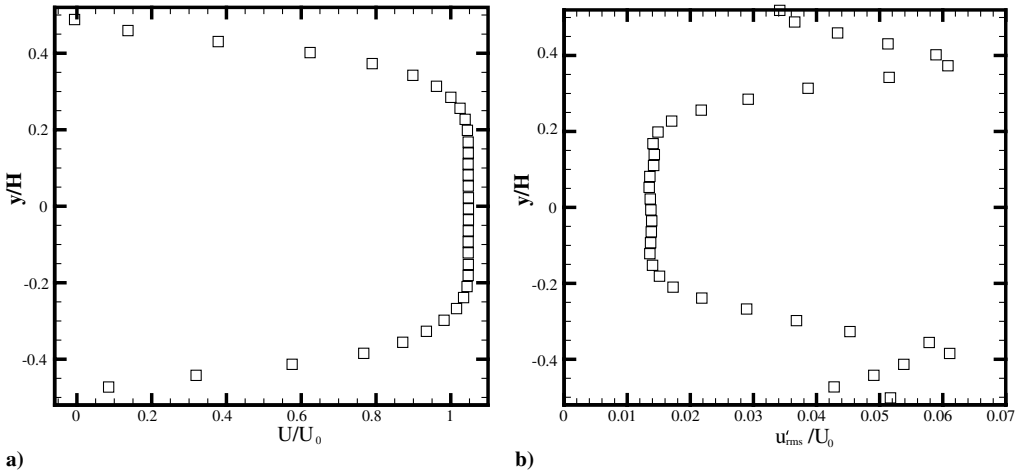


**Fig. 2 Profiles of mean and rms fluctuation in the streamwise velocity near the injection point.**

3 mm thick based on the 99% location and turbulent or transitional near the injection point. The boundary-layer thickness $\delta$ is expected to play a role in the dynamics of the interaction between the jet and main flow. The boundary-layer thickness was not varied in this study, as the objective was to focus on the interaction between suction and injection flow control.

Particle image velocimetry was used to investigate the flowfield inside the test section. For this purpose, the main flow was seeded with olive oil droplets of a nominal diameter of 1 $\mu$m using a Laskin nozzle. The particle illumination was provided by a New Wave Research Solo PIV III Nd:YAG laser capable of 50 mJ/pulse at a rate of 15 Hz. The PIV data was collected at the spanwise midplane of the channel, and the images were processed using $32 \times 32$ pixel interrogation regions with 50% overlap. The interrogation regions are nominally 0.5 mm in the object domain. The velocity computations were done using IDT proVISION-XS software.

A sample set of over 800 image pairs was collected for each case to provide accurate velocity statistics. The uncertainty due to bias and precision error for the instantaneous vector calculations was approximately 0.02 and 0.016 pixels, respectively; the precision error estimate is based on twice the standard deviation as measured for a steady laminar flow, whereas the bias error is extracted from the displacement histograms as described by Roth and Katz [18]. The streamwise mean velocity and standard deviation of the fluctuating velocity had estimated uncertainties due to sample size and flow unsteadiness of 2 and 3.5% of the peak values, respectively.

Several nondimensional parameters were used throughout the study to characterize the fluidics. The suction parameter $C_q$ is defined as the mass flow ratio of suction to primary flow, $C_q = \dot{m}_s/\dot{m}_o$. The momentum ratio $C_\mu$ is used as the parameter for the injection flow control. The momentum ratio has been shown to scale the size of the induced recirculation zone [19] and is defined as

$$C_\mu = \frac{\rho_j U_j^2 d}{\rho_o U_o^2 H} \tag{1}$$

where $j$ and $o$ represent the transverse jet and main flow, respectively, $\rho$ is the density, and $U$ the bulk velocity. This is a first-order parameter and does not incorporate profile shape information. The dimensionless scaling of the recirculation zone height and length found during the present study was in good agreement with the results from Ahmed et al. [20].

The vector angle was calculated using momentum transport derived from PIV data. The transport of streamwise and cross-stream momentum across the channel cross-sectional area were calculated using

$$M_x = \int_y \rho(U^2 + \overline{u'^2})\,\mathrm{d}y \tag{2a}$$

and

$$M_y = \int_y \rho(UV + \overline{u'v'})\,\mathrm{d}y \tag{2b}$$

where $U$ and $V$ correspond to the streamwise and cross-stream mean velocity, respectively, $u'$ and $v'$ are the corresponding turbulent components, and an overbar represents a time average. The vector angle $\alpha$ was calculated at the end of the channel using

$$\alpha = \tan^{-1}(-M_y/M_x) \tag{3}$$

where the negative sign accounts for the fact that the jet vectors downward in the current configuration.

## III. Results

### A. Vectoring Performance

The presentation of the results begins with a general description of the performance of fluidic thrust vectoring using isolated and combined injection and suction. Figure 3 shows the mean streamline pattern for a variety of combinations of suction and injection. The corresponding vector angles are indicated on the figures. Figures 3a and 3b show that the addition of suction in the presence of injection causes an increase in the vector angle, and a modulation of the streamline pattern in the vicinity of the downstream end of the recirculation zone. It is interesting to note that the vector angle achieved with suction and blowing in Fig. 3b is larger than the sum of that achieved with suction and blowing independently, suggesting a constructive interference between the two fluidic vectoring mechanisms. Figures 3b and 3c show the streamline pattern and angle achieved as injection is further increased. The constructive interference is no longer evident, and the ability to vector the jet is degraded. It is apparent that there is a complex interaction between injection and suction for thrust vectoring.

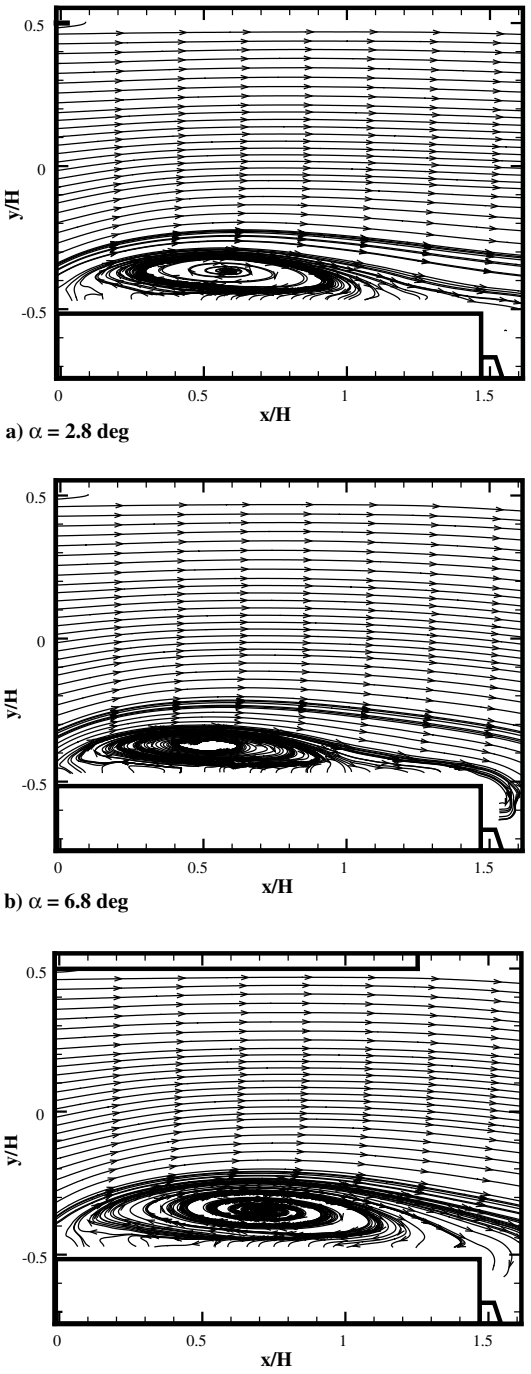


**Fig. 3 Mean streamlines: a) $C_\mu = 0.09$ and $C_q = 0$, b) $C_\mu = 0.09$ and $C_q = 0.07$, and c) $C_\mu = 0.13$ and $C_q = 0.07$.**

Figure 4 shows the vector angle as a function of momentum ratio without the use of suction. The vector angle increases with $C_\mu$,

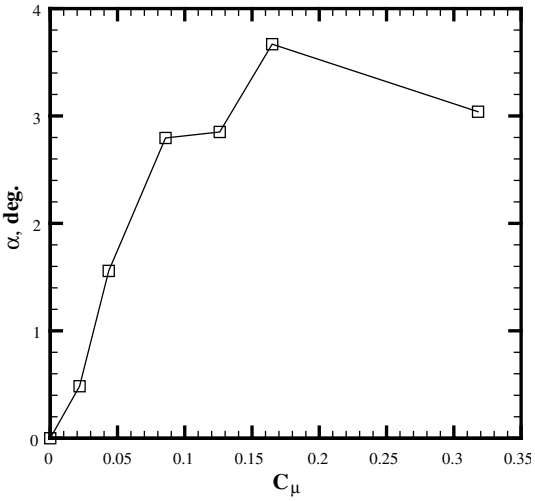


**Fig. 4 Vectoring angle vs momentum ratio.**

although a reduction occurs for the highest $C_\mu$. Note that the recirculation zone size scales monotonically with $C_\mu$ [21]. Because the region of influence caused by injection is expected to scale with the length scale of the recirculation zone, the likely cause for the reduction in angle at high $C_\mu$ is that the recirculation zone is longer than the distance from the injection point to the end of the channel (see Fig. 14). The results suggest that an optimum $C_\mu$ exists at which maximum vector angle is achieved. It is intuitive to expect that the optimum $C_\mu$ will depend on the distance between the injection point and the end of the channel, because the reduction in vector angle appears to be associated with recirculation zones that extend outside the channel.

Figure 5 shows the vector angle for the entire set of conditions considered in the study; note that the vector angle is defined as positive when vectored in the downward direction. Considering first the effect of suction without blowing ($C_\mu = 0$), it is clear that the vector angle has a nonlinear relationship with the suction mass flow rate. The vector angle undergoes rapid growth at higher suction mass flow rates.

At suction rates higher than approximately 10% (not shown in Fig. 5), the jet attached to the external surface of the suction chamber, similar to the attached jet mode observed for counterflow thrust vectoring [22]. Interestingly, it was observed during the present study that the use of injection with high suction tended to suppress jet attachment. As will be shown later, the injection tends to redistribute the momentum flux of the main flow, with higher momentum flux located away from the injection wall. This redistribution provides resistance to the jet attachment to external surfaces, simulating, in a sense, a larger cross-stream distance between the jet and the collar for the counterflow vectoring method. The present results suggest that injection may facilitate the design of more aggressive configurations for the counterflow thrust vectoring technique, including compact designs that would otherwise be plagued with jet attachment.

At moderate injection rates ($0 < C_\mu < 0.05$), the combination of suction and injection tends to provide augmented vectoring in that slightly higher angles are achieved when compared with the addition of the angles induced independently with suction and injection. Beyond a $C_\mu$ of approximately 0.05, the effect of suction starts to degrade. At the highest $C_\mu = 0.32$, suction has a very limited effect on the vector angle, showing an increase of about 1 deg over the range of suction rates considered. A hypothesis on why the influence of suction degrades at high $C_\mu$ will be described later.

### B. Suction-Based Thrust Vectoring

Having described the general performance of injection and/or suction thrust vectoring, an exploration of the operating mechanisms will now be considered. Before discussing the effects of the combined fluidics, analysis of the isolated use of injection and suction will be described.

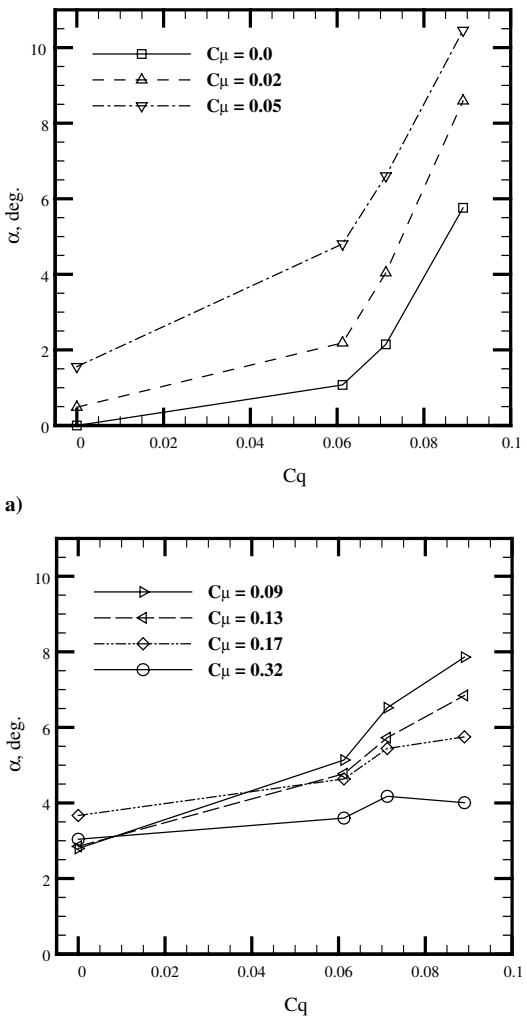


**Fig. 5 Vectoring angle vs suction flow rate for different momentum ratios.**

The employment of suction control will first be documented to understand the operating mechanism. The streamwise evolution of the vertical momentum $M_y$ within the channel for the various suction cases (with no injection) is presented in Fig. 6. Note that the origin of the streamwise coordinate $x/H$ is located at the injection point (an arbitrary location for the pure suction cases). As found for synthetic jet vectoring [23], the application of fluidic control at the exit plane influences the flow inside the channel. A local momentum balance across the channel shows that

$$\Delta P = -\frac{\partial M_y}{\partial x} \tag{4}$$

where $\Delta P$ is the pressure drop from the top to the bottom of the channel. In the absence of local blowing or suction at the walls, the only way a net change in cross-stream momentum can be generated within a channel is through a cross-stream pressure gradient. It can be seen from the figure that the influence of suction is limited to a spatial extent of approximately $1.5H$ upstream of the exit of the channel, in general agreement with other methods that employ pressure boundary condition control [15,23]. The increase in slope of the streamwise momentum with suction mass flow rate is consistent with the increase in vector angle observed in Fig. 5. The zero suction case indicates a small change in cross-stream momentum between the injection point and the exit. This variation is likely caused by asymmetry of the exit boundary conditions and/or the presence of the slot jet that potentially disturbs the boundary layer on the lower wall. The baseline thrust vector angle ($\sim$0.2 deg) was subtracted off all

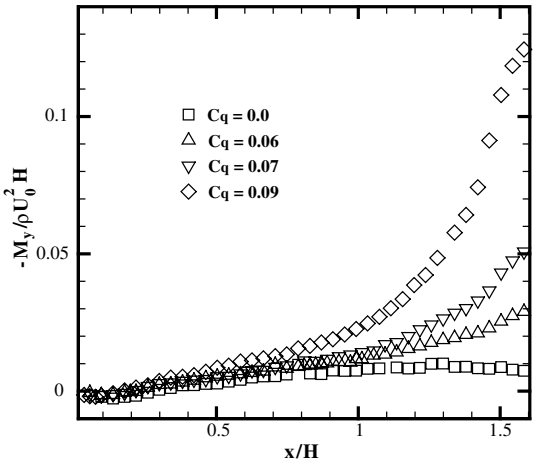


**Fig. 6 Vertical momentum evolution for the suction-only cases.**

measurements to show a relative angle change due to the fluidic control.

Figure 7a presents the mean streamwise velocity at the exit of the channel for no and moderate suction. The manifestation of the altered static pressure distribution at the exit plane of the nozzle is indicated in the skewed streamwise velocity profile. The higher streamwise momentum flux near the lower wall is caused by the lower local static pressure due to the proximity of the suction source.

The mean transverse velocity profiles are shown in Fig. 7b and indicate that the flow within the channel is flowing toward the wall with the suction control. The central region of the channel shows a nominally constant gradient in the mean cross-stream velocity. There is no turbulence augmentation in the channel through the use of suction; hence, the vectoring mechanism is simply the control of the mean flow through alteration of the static pressure distribution near the exit of the channel. The nonzero velocity indicated in the central region for the case without suction is caused by the asymmetry described earlier.

### C. Injection-Based Thrust Vectoring

Having described the operating mechanism of suction-based thrust vector control, focus will now be placed on vectoring using injection only. As mentioned in the Introduction, rectangular transverse jets are a viable method for manipulating the static pressure along the wall. The present configuration is different than the Weston and Thames study [8] in that the spanwise boundary conditions encourage two-dimensional flow. The avoidance of leakage of crossflow fluid around the jet for the present study is expected to enhance the influence of the transverse jet on the static pressure field.

Figure 8 shows the streamwise development of the cross-stream momentum for the various injection cases. The initial region, $x/H < 0.3$, suffers from inadequate spatial resolution due to the small size of the injection jet relative to the PIV interrogation region size. Hence, the $M_y$ values are not accurate in this region. This region will produce a positive $M_y$ (in our coordinate system) due to the positive pressure upstream of the jet and the transverse jet momentum.

Downstream of approximately $x/H = 0.2$, the streamwise development of cross-stream momentum reverses due to the low pressure along the lower channel wall downstream of the jet. As the channel exit is approached, the net transport of cross-stream momentum is negative (downward), indicating that the reduced static pressure field downstream of the injection overcomes the effects of the upstream positive pressure and the positive cross-stream momentum added through the injection process.

The streamwise evolution of the streamwise momentum for the various injection cases is shown in Fig. 9. Note that data near $x/H = 1.15$ were removed due to spurious effects on the PIV data due to a shadow in the laser sheet produced by the downstream edge

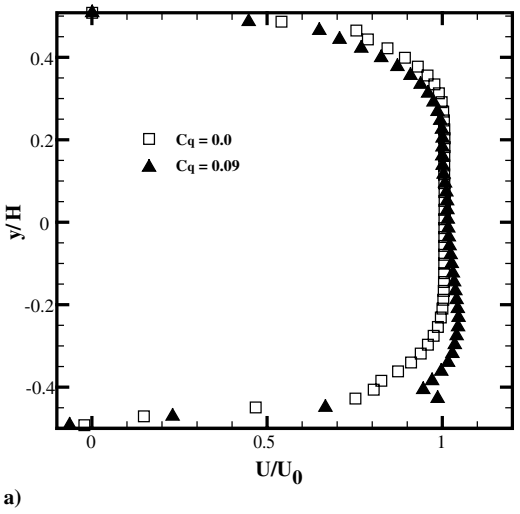


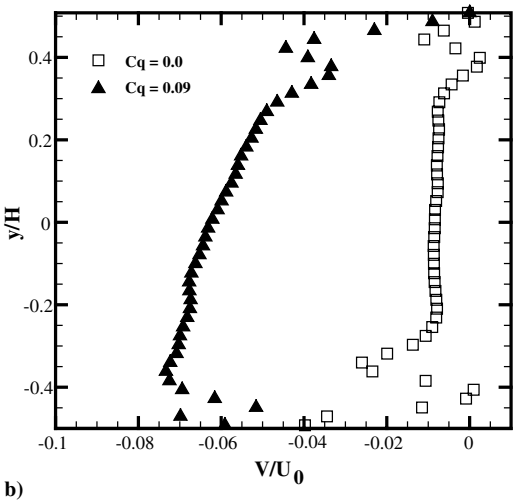


**Fig. 7 Channel exit profiles of mean velocity: a) streamwise, and b) cross stream.**

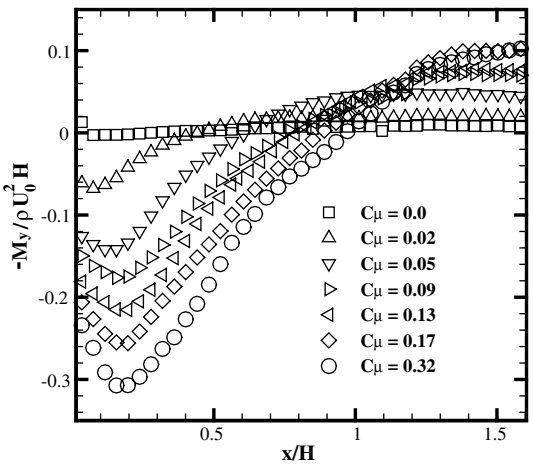


**Fig. 8 Vertical momentum evolution for injection-only cases.**

of the upper channel. It is clear that the streamwise momentum is enhanced due to the injection. In essence, the recirculation zone causes a restriction in the channel flow, requiring acceleration to satisfy mass conservation. Although momentum is increased, the employment of fluidic control on a real propulsion system requires mass flow and power that must be taken into account with respect to any net benefits on the system performance and efficiency. The streamwise momentum peaks near the maximum height of the

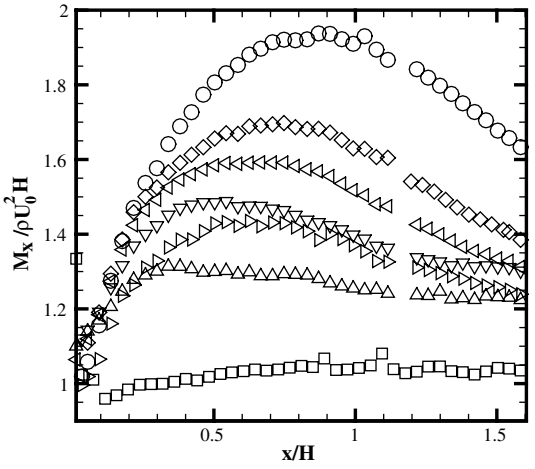


**Fig. 9 Streamwise momentum evolution for injection only.**

induced recirculation zone and decays slowly downstream due to turbulent diffusion. Unlike the suction control case, the exit pressure will be nominally uniform and atmospheric; hence, additional pressure drag may not be incurred with the injection-based method.

It is apparent that fluidic injection is effective at promoting the development of a cross-stream pressure difference [see Eq. (4)]. It has been shown by Ahmed et al. [21] that a significant portion of the recirculation zone induced through transverse injection has characteristics that are similar to free shear layers. Figure 10 shows

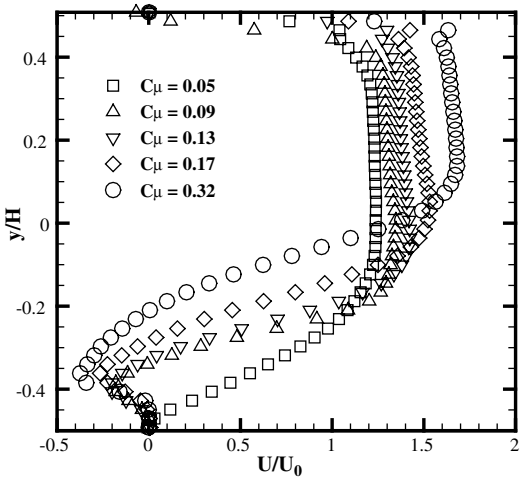


**Fig. 10 Cross-stream profiles at the center of the recirculation zone.**

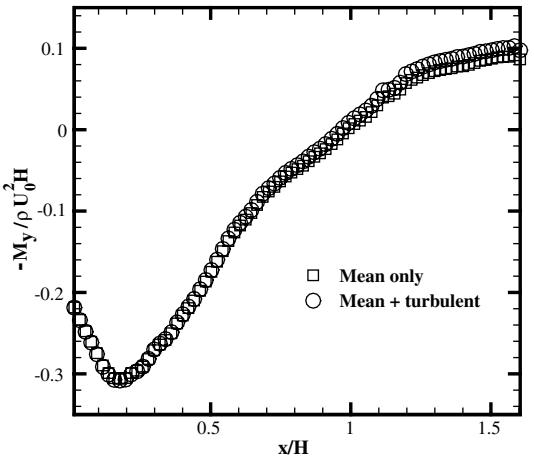


**Fig. 11 Comparison of mean and turbulent momentum contributions to $M_y$.**

the cross-stream profiles of the mean streamwise velocity taken at the center of the recirculation zone for the various injection rates. It is clear in the injection cases that the mean streamwise velocity profile has a similar shape to that of a shear layer that is, in fact, a countercurrent shear layer. Ahmed et al. [21] also found that profiles

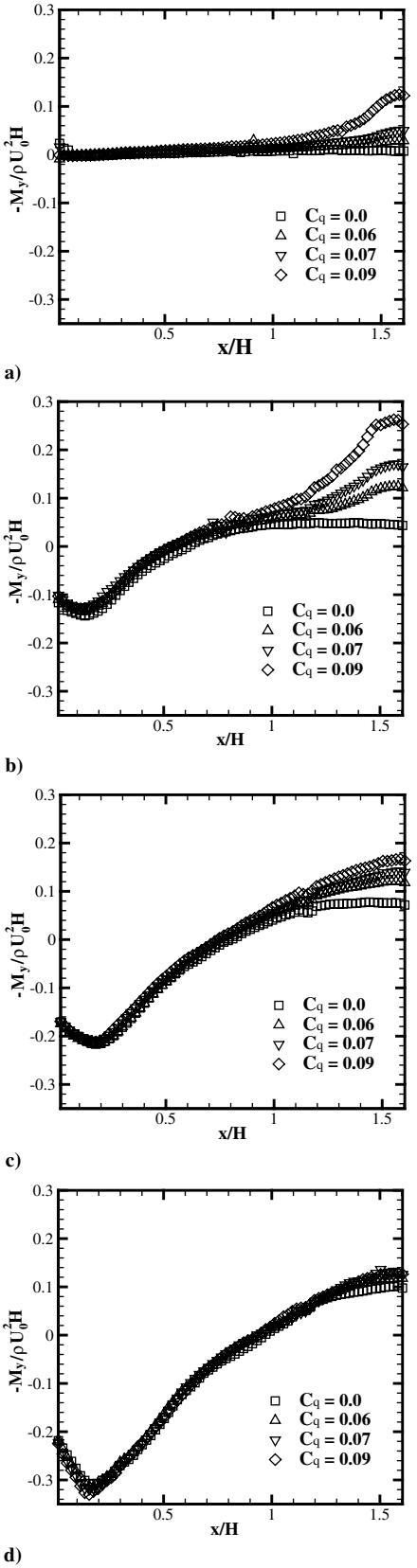


**Fig. 12 Vertical momentum evolution for $C_\mu$ =: a) 0.0, b) 0.05, c) 0.13, and d) 0.32.**

of the Reynolds stresses are quasi symmetric as expected for a shear layer.

The velocity of the freestreams for a shear layer has a profound influence on the shear layer development. The velocity ratio parameter $\lambda$ is defined as

$$\lambda = \frac{U_1 - U_2}{U_1 + U_2} \tag{5}$$

where $U_1$ and $U_2$ are the magnitudes of the faster and slower streams, respectively. The shear layer entrainment model of Dimotakis [24] indicates that the entrainment across a shear layer becomes increasingly asymmetric as $\lambda$ increases from zero. The results of Tang [25] also show that entrainment velocity difference across a shear layer becomes increasingly asymmetric for countercurrent shear layers. The entrainment asymmetry supports the hypothesis that, under confined conditions, it is expected that the countercurrent shear flow plays an important role in establishing a cross-stream pressure difference. Schemes that enhance the countercurrent shear in the recirculation zone may also provide performance benefits.

Some discussion is warranted on the role of turbulence on the establishment of a cross-stream pressure difference. Figure 11 shows the streamwise development of cross-stream momentum with and without the inclusion of the turbulent momentum flux term in Eq. (2b). The actual turbulent flowfield produces a small fraction of the overall cross-stream momentum, reaching about 10% of the total momentum near the channel exit. The results of Fig. 11 indicate that turbulence has a limited *direct* effect on the balancing of cross-stream pressure difference.

Although turbulent momentum flux appears to play a secondary role in balancing the cross-stream pressure drop, turbulence must play an important role in the overall mechanism. Guidance is available through consideration of flow control studies of recirculation zones [26–28], rearward-facing step flows [29–31], and base pressure models for bluff bodies [32]. The common finding in these studies is that excitation of turbulent structures in the separated shear layer alters the mean flow in a significant manner, causing a significant shortening of the recirculation zone. Many of these studies find that enhanced turbulence causes a higher peak vacuum pressure in the recirculation zone, although it is maintained over a shorter distance because the recirculation zone length is reduced. These two trends provide competing effects on the development of cross-stream momentum; therefore, it is not clear if turbulence control applied to the separated flow of the recirculation will produce vectoring performance gains.

An enhanced understanding of the relationships between static pressure, mean flow, and turbulence for this particular flow is required before the mechanism can be optimized, although results to date suggest that vectoring will be maximized for large recirculation zones containing high turbulence levels.

### D. Combined Suction and Injection

Having discussed the separate effects of suction and injection, the combined effects can now be described. As shown in Fig. 5, the effect of combined suction and blowing is complex; the influence of suction is strong at low injection rates and degrades at high injection, with the transition occurring above $C_\mu = 0.05$.

To gain a better understanding of the coupled fluidic vectoring performance, the streamwise evolution of the cross-stream momentum is plotted in Fig. 12 for various momentum ratios and suction rates. A number of observations are made with respect to Fig. 12. The influence of suction is again limited to the downstream end of the test section; hence, suction has no influence on the cross-stream pressure difference in the upstream half of the recirculation zone. Comparing Figs. 12a and 12b, the application of the same level of suction is shown to produce a higher magnitude of $M_y$ for the case with low injection. As the injection is increased (Figs. 12c and 12d),

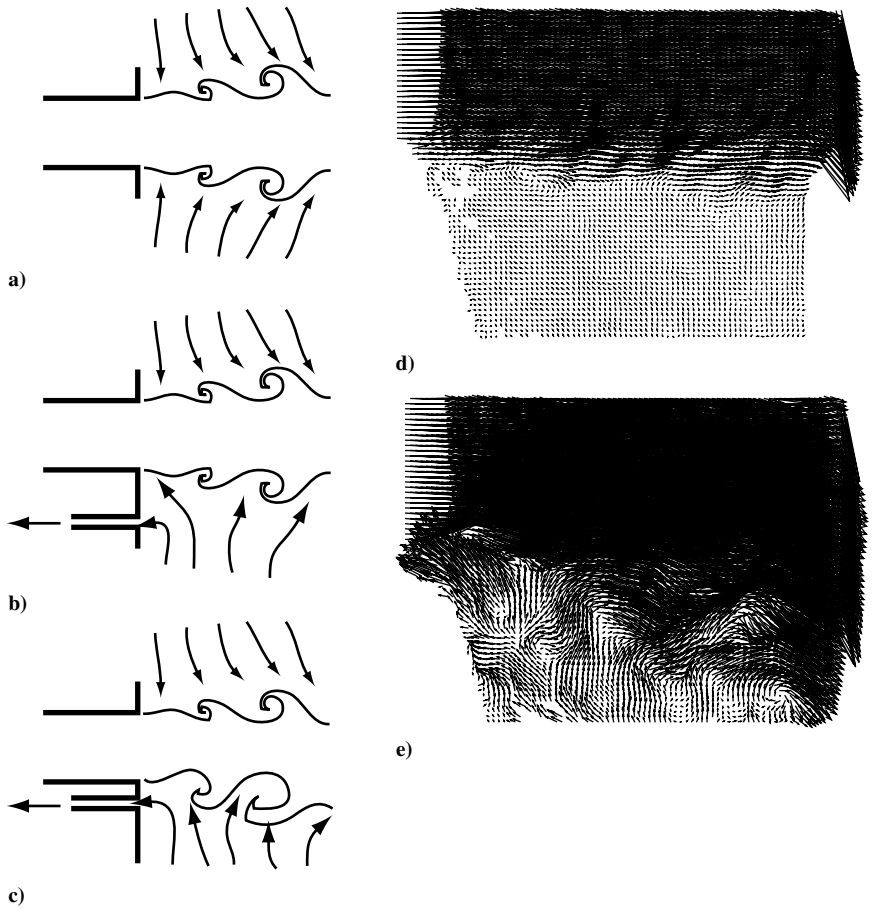


**Fig. 13 Schematic of the entrainment: a) free jet, b) jet with suction entrainment control, and c) jet with countercurrent shear layer control. Instantaneous velocity vector fields: d) no suction, and e) high suction.**

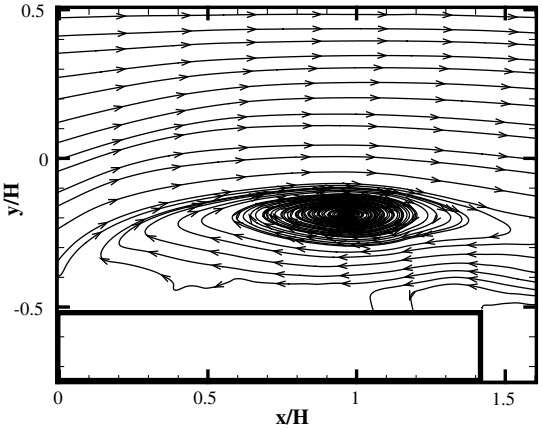


**Fig. 14 Mean streamline pattern for $C_\mu = 0.32$ and $C_q = 0.09$.**

the influence of suction decays until very little additional vertical momentum is produced with the addition of suction.

Suction creates a local reduction in pressure due to the sinklike flowfield. The suction flow can induce changes in the near field of the jet. Figure 13a shows a schematic of the flow outside the channel. The shear layer of the jet induces entrainment of the ambient fluid. This ambient fluid motion is nearly ideal before entering the shear layer; hence, the total pressure is nominally constant up to the outer edge of the shear layer. It is well known that the entrainment induced across a shear layer is governed by the profile of Reynolds shear stress [33–35]. This explains why asymmetric entrainment caused by mixing control techniques results in thrust vector control (e.g., [17]) even under unconfined conditions. If the suction slot is located too far from the jet, as shown in Fig. 13b, the main role of suction with respect to the jet is the redistribution of the entrainment flowfield. Figure 13c is a schematic of the flowfield expected when the suction flow is close enough to result in an interaction between the suction flow and the shear layer of the jet. The suction flow will create a local countercurrent shear layer that causes enhanced growth of the jet shear layer. This enhanced growth will be manifested in enhanced Reynolds shear stresses and higher entrainment rates, features that cause a reduction in local static pressure (relative to the far-field ambient pressure). Figures 13d and 13e show instantaneous vector fields of the jet shear layer under zero and high suction levels, respectively. It is clear that the shear layer is highly disturbed by the application of suction, suggesting that the suction influences shear layer spreading and entrainment as depicted in Fig. 13c. In particular, the entrainment velocity of the ambient fluid is greatly enhanced with the addition of suction, which aids in setting the static pressure boundary condition that acts to vector the jet.

It is apparent from Figs. 5 and 12 that the presence of high levels of injection results in a decreased effectiveness of suction. The streamline pattern for a high injection case is shown in Fig. 14. It is seen that the recirculation zone extends outside the channel, and the unattached recirculation zone results in entrainment of ambient fluid into the channel. The local counterflow of the suction is now located further away from the jet and is unable to excite the shear layer. Suction will have an influence as shown in Fig. 13b, with the overall results of the present study suggesting very weak vector angle enhancement with suction in this regime.

It appears that, for suction to augment vectoring effectively, the shear layer mixing must be enhanced as suction is increased. Figure 15 shows the cross-stream profiles of Reynolds shear stress outside the channel at $x/H = 1.8$ for different levels of suction and injection. In Fig. 15a, it is shown that an increase in suction results in an increase in the peak Reynolds shear stress for zero injection. The shear layer is also visibly thickened at this point due to the application of suction. For the $C_\mu = 0.09$ injection case shown in Fig. 15b, the increase in suction has a very small influence on the Reynolds shear stress. The results overall suggest that suction control is most effective when locally induced countercurrent shear flow can influence the mixing characteristics of the shear layer.

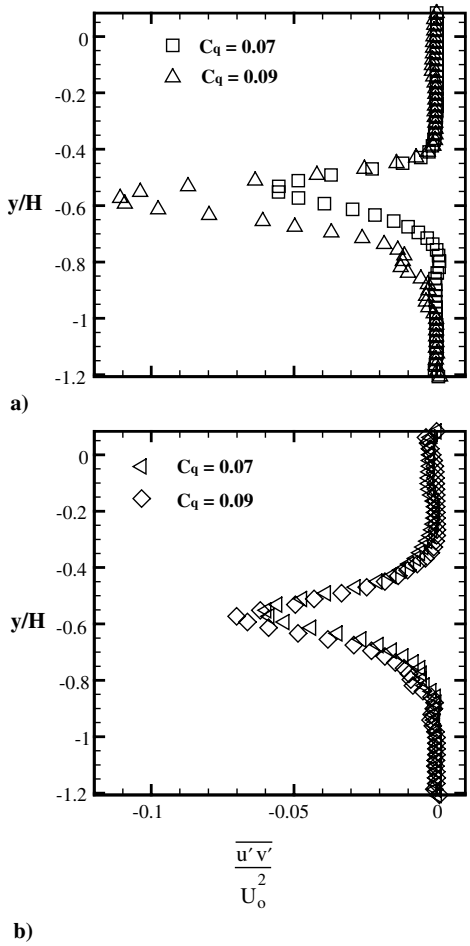


**Fig. 15 Cross-stream profiles of Reynolds shear stress at $x/H = 1.8$: a) $C_\mu = 0.0$, and b) $C_q = 0.09$.**

## IV. Conclusions

A fluidic thrust vectoring concept combining a transverse jet and suction was investigated. The vectoring of the flow issuing from a rectangular channel with a Reynolds number of 39,000 was considered. The two fluidic techniques were varied and the response of the flow was studied. It was noted that at low injection rates the effect of suction on the vectoring was enhanced, whereas suction at high injection experienced a degraded response. The mechanisms of the vectoring for the isolated fluidics were investigated, and it was found that suction alters the static pressure distribution near the jet exit, whereas injection induced a shear flow that would, under unconfined conditions, produce asymmetric entrainment velocities. Suction is effective when the suction flow enhances the entrainment and mixing of the jet shear layer. The vectoring with combined injection and suction was studied, and it was found that suction had enhanced influence on the vector angle at low injection rates, whereas it had a degrading effect at high injection. The degraded effect of suction is associated with a flow regime where the main flow does not reattach within the channel, a scenario in which the suction flow does not disturb the jet shear layer.

## Acknowledgment

The authors would like to express thanks to Kareem Ahmed, who helped with configuring the experiment and the collection and organization of the data.

## References

[1] Wing, D., "Static Investigation of Two Fluidic Thrust-Vectoring Concepts on a Two-Dimensional Convergent-Divergent Nozzle," NASA TM-4574, 1994.

[2] Miller, D. N., Yagle, P. J., and Hamstra, J. W., "Fluidic Throat Skewing for Thrust Vectoring in Fixed-Geometry Nozzles," AIAA Paper 1999-365, 1999.
[3] Deere, K., Berrier, B., Flamm, J., and Johnson, S., "Computational Study of Fluidic Thrust Vectoring Using Separation Control in a Nozzle," AIAA Paper 2003-3803, 2003.
[4] Flamm, J. D., Deere, K. A., Mason, M. L., Berrier, B. L., and Johnson, S. K., "Design Enhancements of the Two-Dimensional, Dual Throat Fluidic Thrust Vectoring Nozzle Concept," AIAA Paper 2006-3701, 2006.
[5] Flamm, J. D., Deere, K. A., Mason, M. L., Berrier, B. L., and Johnson, S. K., "Experimental Study of an Axisymmetric Dual Throat Fluidic Thrust Vectoring Nozzle for Supersonic Aircraft Application," AIAA Paper 2007-5084, 2007.
[6] Mason, S. M., and Crowther, W. J., "Fluidic Thrust Vectoring of Low Observable Aircraft," *CEAS Aerospace Aerodynamic Research Conference*, Confederation of European Aerospace Societies, Cambridge, England, UK, 2002.
[7] Allen, D., and Smith, B. L., "Axisymmetric Coanda-Assisted Vectoring," *Experiments in Fluids*, Vol. 46, No. 1, 2009, pp. 55–64. doi:10.1007/s00348-008-0536-y
[8] Weston, R. P., and Thames, F. C., "Properties of Aspect-Ratio-4. 0 Rectangular Jets in a Subsonic Crossflow," *Journal of Aircraft*, Vol. 16, No. 10, 1979, pp. 701–707. doi:10.2514/3.58592
[9] Yagle, P. J., Miller, D. N., Ginn, K. B., and Hamstra, J. W., "Demonstration of Fluidic Throat Skewing for Thrust Vectoring in Structurally Fixed Nozzles," *Journal of Engineering for Gas Turbines and Power*, Vol. 123, No. 3, 2001, pp. 502–507. doi:10.1115/1.1361109
[10] Strykowski, P. J., and Krothapalli, A., "The Countercurrent Mixing Layer- Strategies for Shear-Layer Control," AIAA Paper 1993-3260, 1993.
[11] Gillgrist, R. D., Forliti, D. J., and Strykowski, P. J., "On the Mechanisms Affecting Fluidic Vectoring Using Suction," *Journal of Fluids Engineering*, Vol. 129, No. 1, 2007, pp. 91–99. doi:10.1115/1.2375125
[12] Alvi, F. S., Strykowski, P. J., Krothapalli, A., and Forliti, D. J., "Vectoring Thrust in Multiaxes Using Confined Shear Layers," *Journal of Fluids Engineering*, Vol. 122, 2000, pp. 3–13. doi:10.1115/1.483220
[13] Santos, M. M., "Experimental Study on Counter Flow Thrust Vectoring of a Gas Turbine Engine," Ph.D. Thesis, Mechanical Engineering Dept., Florida State Univ., Tallahassee, FL, 2005.
[14] Smith, B. L., and Glezer, A., "Vectoring and Small-Scale Motions Effected in Free Shear Flows Using Synthetic Jet Actuators," AIAA Paper 1997-213, 1997.
[15] Bettridge, M. W., Smith, B. L., and Spall, R. E., "Aerodynamic Jet Steering Using Steady Blowing and Suction," *Experiments in Fluids*, Vol. 40, No. 5, 2006, pp. 776–785. doi:10.1007/s00348-006-0115-z
[16] Humes, Z. E., and Smith, B. L., "Particle Size Classification of Glass Particles Using Aerodynamic Jet Vectoring," *Particle and Particle Systems Characterization*, Vol. 25, No. 2, 2008, pp. 168–175. doi:10.1002/ppsc.200700019
[17] Lim, D. W., and Redekopp, L. G., "Aerodynamic Flow-Vectoring of a Planar Jet in a Co-Flowing Stream," *Journal of Fluid Mechanics*, Vol. 450, 2002, pp. 343–375.doi:10.1017/S0022112001006462
[18] Roth, G. I., and Katz, J., "Five Techniques for Increasing the Speed and Accuracy of PIV Interrogation," *Measurement Science and Technology*, Vol. 12, No. 3, 2001, pp. 238–245. doi:10.1088/0957-0233/12/3/302
[19] Ahmed, K. A., Forliti, D. J., Moody, J. K., and Yamanaka, R., "Flowfield Characteristics of a Confined Transverse Slot Jet," *AIAA Journal*, Vol. 46, No. 1, 2008, pp. 94–103. doi:10.2514/1.29799
[20] Ahmed, K., Moody, J., and Forliti, D. J., "The Effect of Slot Jet Size on the Confined Transverse Slot Jet," *Experiments in Fluids*, Vol. 45, No. 1, 2008, pp. 13–26. doi:10.1007/s00348-008-0461-0
[21] Ahmed, K., Moody, J., and Forliti, D. J., "The Effect of Slot Jet Size on the Confined Transverse Slot Jet," *Experiments in Fluids*, Vol. 45, No. 1, 2008. pp. 13–26. doi:10.1007/s00348-008-0461-0
[22] Van der Veer, M. R., and Strykowski, P. J., "Counterflow Thrust Vector Control of Subsonic Jets: Continuous and Bistable Regimes," *Journal of Propulsion and Power*, Vol. 13, No. 3, 1997, pp. 412–420. doi:10.2514/2.5179
[23] Smith, B. L., and Glezer, A., "Jet Vectoring Using Synthetic Jets," *Journal of Fluid Mechanics*, Vol. 458, 2002, pp. 1–34. doi:10.1017/S0022112001007406
[24] Dimotakis, P. E., "Two-Dimensional Shear-Layer Entrainment," *AIAA Journal*, Vol. 24, No. 11, 1986, pp. 1791–1796. doi:10.2514/3.9525
[25] Tang, B. A., "An Experimental Investigation of Planar Countercurrent Turbulent Shear Layers," Masters Thesis, Mechanical Engineering Dept., Univ. of Minnesota, Minneapolis, MN, 2002.
[26] Kiya, M., Shimizu, M., and Mochizuki, O., "Sinusoidal Forcing of a Turbulent Separation Bubble," *Journal of Fluid Mechanics*, Vol. 342, 1997, pp. 119–139. doi:10.1017/S0022112097005521
[27] Halfon, E., Nishri, B., Seifert, A., and Wygnanski, I., "Effects of Elevated Free-Stream Turbulence on Actively Controlled Separation Bubble," *Journal of Fluids Engineering*, Vol. 126, No. 6, 2004, pp. 1015–1024. doi:10.1115/1.1839933
[28] Greenblatt, D., and Wygnanski, I. J., "The Control of Flow Separation by Periodic Excitation," *Progress in Aerospace Sciences*, Vol. 36, No. 7, 2000, pp. 487–545. doi:10.1016/S0376-0421(00)00008-7
[29] Chun, K. B., and Sung, H. J., "Control of Turbulent Separated Flow Over a Backward-Facing Step by Local Forcing," *Experiments in Fluids*, Vol. 21, No. 6, 1996, pp. 417–426.doi:10.1007/BF00189044
[30] Yoshioka, S., Obi, S., and Masuda, S., "Turbulence Statistics of Periodically Perturbed Separated Flow Over Backward-Facing Step," *International Journal of Heat and Fluid Flow*, Vol. 22, No. 4, 2001, pp. 393–401. doi:10.1016/S0142-727X(01)00079-0
[31] Forliti, D. J., and Strykowski, P. J., "Controlling Turbulence in a Rearward-Facing Step Combustor Using Countercurrent Shear," *Journal of Fluids Engineering*, Vol. 127, No. 3, 2005, pp. 438–448. doi:10.1115/1.1899170
[32] Tanner, M., "Theories for Base Pressure in Incompressible Steady Base Flow," *Progress in Aerospace Sciences*, Vol. 34, No. 7–8, 1998, pp. 423–480. doi:10.1016/S0376-0421(98)00007-4
[33] Forliti, D. J., Tang, B. A., and Strykowski, P. J., "An Experimental Investigation of Planar Countercurrent Turbulent Shear Layers," *Journal of Fluid Mechanics*, Vol. 530, 2005, pp. 241–264. doi:10.1017/S0022112005003642
[34] Browand, F. K., and Latigo, B. O., "Growth of the 2-Dimensional Mixing Layer from a Turbulent and Non-Turbulent Boundary-Layer," *Physics of Fluids*, Vol. 22, No. 6, 1979, pp. 1011–1020. doi:10.1063/1.862705
[35] Liepmann, H. W., and Laufer, J., "Investigations of Free Turbulent Mixing," NACA TN-1257, 1947.

M. Glauser
*Associate Editor*